

EVIDENCE FOR TIDAL STRIPPING OF DARK MATTER HALOS IN MASSIVE CLUSTER-LENSES

PRIYAMVADA NATARAJAN¹, JEAN-PAUL KNEIB² & IAN SMAIL³

¹ Department of Astronomy, Yale University, New Haven, CT, USA

² Observatoire Midi-Pyrenees, 14 Av. E.Belin, 31400 Toulouse, France

³ Department of Physics, University of Durham, South Road, Durham DH1 3LE, UK

Draft version November 7, 2018

ABSTRACT

In this letter, we present the results of our study of galaxy-galaxy lensing in massive cluster-lenses spanning $z = 0.17$ to 0.58 , utilizing high-quality archival *Hubble Space Telescope* (*HST*) data. Local anisotropies in the shear maps are assumed to arise from dark matter substructure within these clusters. Associating the substructure with bright early-type cluster galaxies, we quantify the properties of typical L^* cluster members in a statistical fashion. The fraction of total mass associated with individual galaxies within the inner regions of these clusters ranges from 10–20% implying that the bulk of the dark matter in massive lensing clusters is smoothly distributed. Looking at the properties of the cluster galaxies, we find strong evidence ($> 3\text{-}\sigma$ significance) that a fiducial early-type L^* galaxy in these clusters has a mass distribution that is tidally truncated compared to equivalent luminosity galaxies in the field. In fact, we exclude field galaxy scale dark halos for these cluster early-types at $> 10\text{-}\sigma$ significance. We compare the tidal radii obtained from this lensing analysis with the central density of the cluster potentials and find a correlation which is in excellent agreement with theoretical expectations of tidal truncation: $\log[r_{t*}] \propto (-0.6 \pm 0.2) \log[\rho_0]$.

Subject headings: gravitational lensing, galaxies: fundamental parameters, halos, methods: numerical

1. INTRODUCTION

Galaxy-galaxy lensing provides a powerful tool to statistically measure the mass and the details of the mass distribution for field galaxies (Tyson et al. 1984; Brainerd et al. 1996). These studies confirm the existence of massive dark matter halos around typical field galaxies, extending to beyond 100 kpc^1 (Brainerd et al. 1996; Fischer et al. 2000; Smith et al. 2001b; McKay et al. 2001). The same technique can be modified and implemented within clusters to constrain the masses of cluster galaxies (Natarajan & Kneib 1997, NK97; Geiger & Schneider 1998). Successful application of the same to the rich, lensing cluster AC114 at $z = 0.31$, suggests that the average M/L ratio and spatial extents of the dark matter halos associated with early-type galaxies in such dense environments may differ from those of comparable luminosity field galaxies (Natarajan et al. 1998, NKSE98).

The technique applied by NKSE98 quantifies the local weak distortions in the observed shear field of massive cluster-lenses, as perturbations arising from the massive halos of cluster galaxies (for details see NK97). By associating these perturbations with bright early-type cluster members, the relative mass fraction in their halos is constrained using a combined χ^2 -maximum likelihood method. The strength of this approach is the simultaneous use of constraints from the observed strong and weak lensing features.

The fractional mass in clusters associated with individual galaxy halos has important consequences for the

frequency and nature of interactions (Moore et al. 1996; Ghigna et al. 1998; Okamoto & Habe 1999; Merritt 1983). The theoretical expectation is that the global tidal field of a massive, dense cluster potential well should be strong enough to truncate the dark matter halos of galaxies that traverse the cluster core. In this letter, we test this expectation using well calibrated mass models for rich clusters at $z \sim 0.17\text{--}0.58$ that utilize the observed strong lensing features – positions, magnitudes, geometry of multiple images and measured spectroscopic redshifts as well as the shear field.

2. GALAXY-GALAXY LENSING IN CLUSTERS

The clusters in our study are modeled as a superposition of a smooth large-scale potential and smaller scale potentials that are associated with bright early-type cluster members: $\phi_{\text{tot}} = \phi_{\text{clus}} + \sum_i \phi_{\text{p}_i}$, where ϕ_{clus} is the potential of the smooth component and ϕ_{p_i} are the potentials of the perturbers (galaxy halos). The resultant reduced shear g , 2 , g , and can in turn be decomposed into contributions from the smooth clump and perturbers.

To quantify the lensing distortion induced by ϕ_{tot} , the smooth cluster piece and individual galaxy-scale halos are modeled self-similarly using the pseudo-isothermal elliptical (PIEMD) surface density profile, $\Sigma(R)$ derived by Kasiola & Kovner (1993), with a core-radius r_0 , a truncation radius $r_t \gg r_0$ and an ellipticity ϵ . These parameters are tuned for both the smooth component and the perturbers to obtain mass distributions on the relevant scales

¹We adopt $h=H_0/100 \text{ km s}^{-1} \text{ Mpc}^{-1}=0.5$ and $q_o = 0.5$, $\Omega_o = 1$. Our results however, are not sensitive to values of the cosmological parameters.

²The reduced shear g , a complex number, is defined in terms of the convergence κ and the shear γ , as $g = \gamma/(1 - \kappa)$, can be directly related to the measured shape parameter $\tau = 2g/(1 - g^*g)$

(for details see §2.2 of NK97). Note that r_t characterizes the scale over which the local potential dominates. Additionally, assuming light traces mass, the light distribution of the early-type cluster members is related to the mass model via a set of the usual adopted scaling laws motivated by observations (see Brainerd et al. 1996):

$$\sigma_0 = \sigma_* \left(\frac{L}{L_*}\right)^{\frac{1}{4}}; r_0 = r_{0*} \left(\frac{L}{L_*}\right)^{\frac{1}{2}}; r_t = r_{t*} \left(\frac{L}{L_*}\right)^{\frac{1}{2}}. \quad (1)$$

The effect of these assumed scaling laws on the maximum-likelihood analysis has been explored in detail using simulations in NK97. The total mass M and the total mass-to-light ratio M/L of cluster galaxies then scales as follows:

$$M \propto \sigma_*^2 r_{t*} \left(\frac{L}{L_*}\right); \frac{M}{L} \propto \sigma_*^2 r_{t*}. \quad (2)$$

The ellipticity of the mass clumps is set to the observed ellipticity of each cluster galaxy. Since, we are sensitive to the induced local shear arising due to the integrated mass within r_t for the clumps, we are not sensitive to details of the assumed radial fall-off and the assumed inner slope of the profile in the galaxy model.

The measured local shear signal in the cluster at the location of the i -th perturber is boosted in value due to two effects (i) the contribution from the smooth cluster component $-\gamma_c$ in the numerator, and (ii) the $(\kappa_c + \kappa_{p_i})$ term in the denominator, which is positive and non-negligible in the central cluster region. By taking into account a smooth cluster model it is possible to reduce the error in the measured shear from the cluster members:

$$\langle g_I - g_c \rangle = \left\langle \frac{\gamma_{p_i}}{1 - \kappa_c - \kappa_{p_i}} \right\rangle, \quad (\sigma_{g_I - g_c}^2) = \frac{\sigma_{g_S}^2}{2} \approx \frac{\sigma_{p(\tau_S)}^2}{N_{bg}},$$

where g_I, g_S and g_c are the shapes of the lensed image (I), unlensed source (S) and the shear of the smooth cluster piece; $\sigma_{p(\tau_S)}^2 \sim 0.3$ is the width of the intrinsic ellipticity distribution of the sources, and N_{bg} the number of background galaxies averaged over. Therefore, knowledge of a well calibrated strong lensing model makes the study of galaxy-galaxy lensing in clusters very viable.

A maximum-likelihood method is used to obtain significance bounds on fiducial parameters that characterize a typical L^* halo in the cluster. We have extended the formalism developed in NK97 to include the strong lensing data for the inner regions of the clusters, these are used to obtain the best model χ^2 fit followed by a likelihood method that incorporates the constraints from the smoothed shear field.

The likelihood function of the estimated probability distribution of the source ellipticities is maximized for a set of model parameters, given a functional form of the intrinsic ellipticity distribution measured for faint galaxies. The entire inversion procedure to solve the lensing equation is performed for each cluster within the LENSTOOL utilities³. Using a well-determined ‘strong lensing’ model for the inner-regions of the clusters along with the averaged shear field and assuming a known functional form for $p(\tau_S)$ from the field, the likelihood for a guessed model is computed using: $\tau_{S_j} = \tau_{\text{obs}_j} - \sum_i^{N_c} \gamma_{p_i} - \gamma_c$ for each faint

galaxy j where $\sum_i^{N_c} \gamma_{p_i}$ is the sum of the shear contribution from N_c perturbers, and γ_c is the shear induced by the smooth component.

$$\mathcal{L}(\sigma_*, r_{t*}) = \prod_j^{N_{gal}} p(\tau_{S_j}). \quad (3)$$

We compute \mathcal{L} assigning the median redshift corresponding to the observed source magnitude for each arclet (details of this procedure can be found in NK97). The best fitting model parameters are then obtained by maximizing the log-likelihood function l with respect to the chosen set of model parameters (σ_*, r_{t*}) and the cluster parameters are simultaneously matched in an iterative way.

3. THE HST CLUSTER-LENSES

For our analysis we select clusters at $z > 0.1$ for which deep, high-quality *HST* imaging is available and which contain spectroscopically-confirmed multiply-imaged high redshift galaxies. These lensed features are essential to construct a detailed mass distribution for the cluster cores (e.g. Kneib et al. 1996; Smith et al. 2001a), while the existence of spectroscopic redshifts allows us to calibrate these mass distributions onto an absolute scale. This selection yields five clusters with redshifts spanning $z = 0.17$ – 0.58 for our analysis: A 2218, A 2390, C1 2244–02, C10024+16, and C10054–27. In addition to these five clusters, we also include our previous analysis of the $z = 0.31$ cluster AC 114 (NKSE98). Details of the cluster properties are given in Table 1 – clearly these clusters do not constitute a well-defined sample, for example their X-ray luminosities span an order of magnitude and their central mass densities show a similarly large dispersion. It is this latter property which is of most interest for our analysis – and the large range spanned by the sample therefore provides a powerful test of the variation in characteristics of galaxy halos with local environment.

The five new clusters were observed with *WFPC2*, four through the F814W (*I*) passband, with A 2218 imaged in F702W (*R*), the total exposure times are listed in Table 1. These typically comprise stacks of multiple single-orbit (2.1–2.7 ks) exposures, each of which is spatially offset by an integer number of *WFC* pixels to allow the removal of cosmic-rays and other artifacts. The data were pipeline processed by STScI and combined using standard STSDAS and IRAF routines. For more details of the reduction see: A 2218, Kneib et al. (1996); A 2390, Pelló et al. (1999); C10024+16 and C10054–27, Smail et al. (1997). These fields reach typical 5- σ detection limits for point sources of $I \sim 26$ or $R \sim 26.5$.

Object catalogs and attendant shape information for faint galaxies are obtained using the SExtractor package (Bertin & Arnouts 1996) and detection criteria of 12 *WFC* pixels above the μ_R or $\mu_I = 25.0$ mag arcsec⁻² isophote after convolution with a 0.3'' diameter top-hat filter. Selection of the background galaxies in these images employs a simple magnitude cut as previously used by NKSE98, either $R = 23$ – 26 or $I = 22.5$ – 25.5 – this provides catalogs of typically ~ 300 – 400 faint galaxies in each field. The magnitude limits employed should select field galaxies at median redshifts of $z \sim 1$, well beyond the clusters. Visual morphological classifications of the

³A fully analytical ray-tracing routine developed by Kneib (1993)

brighter galaxies in these fields, used to select the early-type cluster galaxies, comes from Smail et al. (1997, 2001).

In addition to the strong lens model of AC114 employed by NKSE98, lens models for three of the other clusters have been published previously: A 2218, Kneib et al. (1996); A 2390, Pelló et al. (1999); Cl0024+16, Smail et al. (1996). For the remaining two lenses Cl2244–02 and Cl0054–27, we construct well constrained mass models. The mass distribution in Cl2244–02 has significant substructure, with the main clump centered around the brightest cluster galaxy with a velocity dispersion of $600 \pm 80 \text{ km s}^{-1}$, an ellipticity of 0.17 ± 0.1 and the secondary clump offset about 20 arcseconds away with a velocity dispersion of $300 \pm 40 \text{ km s}^{-1}$ and an ellipticity of 0.1 ± 0.05 . The cluster Cl0054–27 by contrast has a smooth, but extended mass distribution (with a cut-off radius of about $900 \pm 60 \text{ kpc}$) with a central velocity dispersion of $1100 \pm 100 \text{ km s}^{-1}$ and an ellipticity of 0.1 ± 0.05 .

4. RESULTS

Before discussing the results, we describe the various tests we have employed to confirm their reliability. In order to check the authenticity of the signal the following null tests were performed in the likelihood analysis for every cluster: (i) randomizing the positions of the background galaxies, (ii) randomizing the orientations of the background galaxies, and (iii) scrambling the positions of cluster galaxies. No significant maxima were obtained in the likelihood prescription for any of these tests in any of the clusters. To quantify the errors on our derived parameters we note that the principal sources of error in the above analysis are (i) shot noise – we are inherently limited by the finite number of sources sampled within a few tidal radii of each lensing cluster galaxy (in the present analysis we typically have 40 cluster members and ~ 400 background sources); (ii) the spread in the intrinsic ellipticity distribution of the source population; (iii) the unknown source redshifts and (iv) observational errors arising from uncertainties in the measurement of ellipticities from the images for the faintest objects. From simulations where the detailed mass distribution of clusters is known, we have calibrated the sources of error and find that of the above-mentioned four factors, shot noise (accounts typically for $\sim 50\%$ of the incurred error) and the unknown redshifts for individual background galaxies (contributes $\sim 0\text{--}30\%$ depending on the redshift of the cluster) dominate the error budget. The remaining $\sim 20\%$ of the error budget arises due to inaccuracies in the measurement of shapes.

We show in Fig. 1 the likelihood contours for the galaxy perturber models of each of the five clusters. In all cases we detect an unambiguous galaxy-galaxy lensing signal at the $>3\text{-}\sigma$ level – confirming the existence of truncated dark halos associated with early-type galaxies in clusters. The likelihood analysis yields best-fit model parameters: σ^* the central velocity dispersion and truncation radius r_t^* for a typical L^* cluster member, these values are listed in Table 1.⁴ The mass-to-light ratios quoted here take passive evolution of the stellar content of elliptical/S0 galaxies into account modeled using the stellar population synthesis models of Bruzual & Charlot (1993).

⁴The mass obtained for a typical bright cluster galaxy by Tyson et al. (1998) using only strong lensing constraints inside the Einstein radius of the cluster Cl0024+16 is consistent with our results.

5. DISCUSSION AND CONCLUSIONS

We have statistically extracted characteristic parameters for typical L^* cluster galaxies that inhabit massive, dense lensing cluster-lenses ranging in redshift from 0.17–0.58. This has been achieved by combining strong and weak lensing *HST* observations in conjunction with an assumed parametric mass model. We find that the inferred mass distribution of a fiducial L^* is extremely compact, although the inferred r_t^* 's lie well outside the optical radii and correspond to roughly between $5\text{--}10 R_e$. Our analysis also shows that the halos of individual cluster galaxies contribute at most 10–20% of the total mass of the cluster within the central 1 Mpc, covered by the *HST WFPC2* imaging using the results of our likelihood analysis along with the best-fit parameters that characterize the smooth clump. Therefore, in the inner regions of these clusters the bulk of the dark matter is in fact smoothly distributed. Similar lensing studies of field galaxies, e.g. Wilson et al. (2001), typically find a non-zero signal for the radially averaged stacked tangential shear out to 200 kpc. In contrast our study of the halos of galaxies in clusters detects a finite r_t^* , which we attribute to the tidal truncation induced by the motion of these cluster galaxies inside the potential well. From the contours in the likelihood plots, the presence of field galaxy scale dark halos can, in fact, be excluded at $>10\text{-}\sigma$ significance.

The clusters we study here are all rich systems spanning a range in central density, which may explain why the best-fit values of r_t^* obtained vary by a factor of 2–3. To test this suggestion we plot in Fig. 2 the variation of the central density of the cluster dark matter with r_t^*/σ^* based on our lens models and evaluated at the cluster core radius. We see a good correlation and derive a best-fit slope of -0.6 ± 0.2 . This compares well with the theoretical expected value from a tidal stripping model (Merritt 1983) of -0.5 :

$$r_t^* \approx 40 \left(\frac{\sigma_*}{180 \text{ km s}^{-1}} \right) \left(\frac{\rho_0(r_c)}{3.95 \times 10^6 M_\odot \text{ kpc}^{-3}} \right)^{-\frac{1}{2}} \text{ kpc} (4)$$

Dark halos of the scale detected here indicate a high probability of galaxy encounters over a Hubble time within a rich cluster. However, since the internal velocity dispersions of these cluster galaxies ($< 250 \text{ km s}^{-1}$) are much smaller than their orbital velocities, these interactions are unlikely to lead to mergers, suggesting that the encounters of the kind simulated in the ‘galaxy harassment’ picture (Moore et al. 1996) are frequent and likely. In fact, high resolution cosmological N-body simulations of cluster formation and evolution (Ghigna et al. 1998; Moore et al. 1996), find that the dominant interactions are between the global cluster tidal field and individual galaxies after $z = 2$. The cluster tidal field significantly tidally strips galaxy halos in the inner 0.5 Mpc and the radial extent of the surviving halos is a strong function of their distance from the cluster center. Much of this modification is found to occur between $z = 0.5\text{--}0$. Detailed comparison of these results with tidal stripping of dark matter halos in cosmological N-body simulations will be presented in a forthcoming paper.

The prospects for extending this technique to larger scales within clusters in order to study the efficiency of halo stripping as a function of radius (variation of r_t^* as a function of radius) and morphological type are very promising with new instruments such as the *Advanced Camera for Survey* on *HST*. Multi-band imaging will enable photometric redshift determination for the background sources

which will reduce one of the significant sources of noise for future analyses.

PN acknowledges support from Trinity College, Cambridge for a Research Fellowship, JPK from the CNRS and the TMR-Lensing collaboration and IRS from the Royal Society and the Leverhulme Trust.

REFERENCES

- Bernardi, M., et al., [SDSS] 2002, preprint, astro-ph/0110344
 Bertin, E., Arnouts, S., 1996, A&A, 117, 393
 Brainerd, T.G., Blandford, R.D., Smail, I., 1996, ApJ, 466, 623
 Bruzual, G., Charlot, S., 1993, ApJ, 405, 538
 Fischer et al., 2000, AJ, 120, 1198
 Geiger, B., & Schneider, P., 1998, MNRAS, 295, 497
 Ghigna, S., Moore, B., Governato, F., Lake, G., Quinn, T., Stadel, J., 1998, MNRAS, 300, 146
 Kassiola, A., Kovner, I., 1993, ApJ, 417, 450
 Kelson, D., et al., 1997, ApJ, 478, L18
 Kneib, J-P., 1993, PhD thesis, Paul Sabatier University, Toulouse, France
 Kneib, J-P., Ellis, R.S., Smail, I., Couch, W.J., Sharples, R.M., 1996, ApJ, 471, 643
 McKay, T., et al., 2001, preprint, submitted (astro-ph/0108013).
 Merritt, D., 1983, ApJ, 264, 24
 Moore, B., Katz, N., Lake, G., Dressler, A., Oemler, A., 1996, Nature, 379, 613
 Natarajan, P., Kneib, J-P., 1997, MNRAS, 287, 833 [NK97]
 Natarajan, P., Kneib, J-P., Smail, I., Ellis, R.S., 1998, ApJ, 499, 600 [NKSE98]
 Okamoto, T., Habe, A., 1999, ApJ, 516, 591
 Pelló, R., et al., 1999, A&A, 343, L65
 Smail, I., Dressler, A., Kneib, J-P., Ellis, R.S., Couch, W.J., Sharples, R.M., 1996, ApJ, 471, 643
 Smail, I., Dressler, A., Couch, W.J., Ellis, R.S., Oemler, A., Butcher, H., Sharples, R.M., 1997, ApJS, 110, 213
 Smail, I., et al., 2001, ApJ, 323, 839
 Smith, G.P., et al., 2001a, ApJ, 552, 493
 Smith, D.R., Bernstein, G., Fischer, P., Jarvis, M., 2001b, ApJ, 551, 643
 Treu et al., 2002, ApJ, 564, L13
 Tyson, J.A., Valdes, F., Jarvis, J.F., Mills, A.P., 1984, ApJ, 281, L59
 Wilson, G., Kaiser, N., Luppino, G.A., Cowie, L.L., 2001, ApJ, 555, 572

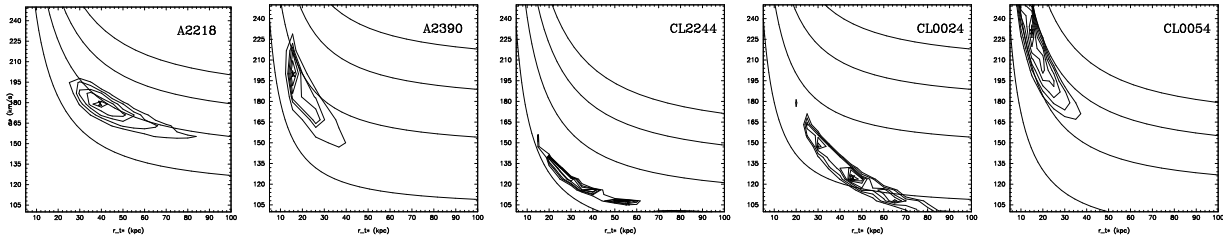


FIG. 1.— The results of the maximum-likelihood analysis for the *HST* cluster-lenses in our sample, σ^* and r_t^* correspond respectively to the central velocity dispersion and outer scale radius (identified as the tidally truncated radius) for a fiducial L^* cluster galaxy in each of these clusters. The contours start at $1-\sigma$ and increase in $1-\sigma$ increments from inside out in all 5 panels. The thick solid lines represent the contours of constant aperture mass and the best-fit values at marked by the cross.

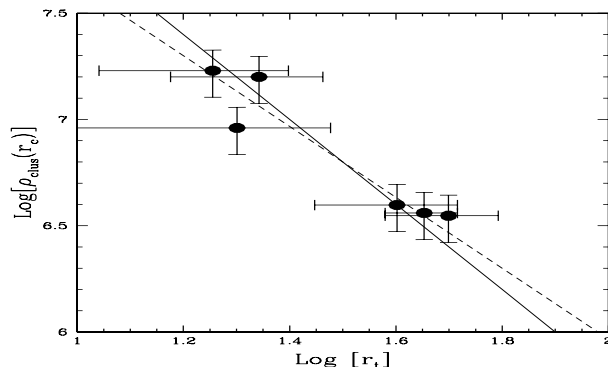


FIG. 2.— Scaling out the variation in the σ^* 's (as per eqn. 4 above), the central density of the cluster evaluated at the core radius is plotted against the tidal radius. The errors plotted in r_t are the $3-\sigma$ values. Performing a least-squares fit to the data points, the value of the best-fit power-law index η , where $r_t^* \propto \rho^\eta$, is estimated to be -0.6 ± 0.2 , (dashed line) in excellent agreement with theoretical expectations of $\eta = -0.5$ (solid line).

Cluster	z	L_X (10^{44} ergs s $^{-1}$)	T_{exp} (ks)	σ^* (km s $^{-1}$)	r_t^* (kpc)	M_{ap}/L_v (M_{\odot}/L_{\odot})	M^* ($10^{11}M_{\odot}$)	σ_{clus} (km s $^{-1}$)	r_c (kpc)	$\rho_{\text{clus}}(r_c)$ ($10^6 \odot \text{kpc}^{-3}$)
A 2218	0.17	9.5	6.3	180 ± 10	40 ± 12	5.8 ± 1.5	~ 14	1070 ± 70	75 ± 10	3.95
A 2390	0.23	23.4	10.5	200 ± 15	18 ± 5	4.2 ± 1.3	~ 6.4	1100 ± 80	55 ± 10	16.95
AC 114	0.31	13.4	16.8	192 ± 35	17 ± 5	6.2 ± 1.4	~ 4.9	950 ± 50	45 ± 15	9.12
Cl 2244-02	0.33	4.8	10.5	110 ± 7	55 ± 12	3.2 ± 1.2	~ 6.8	600 ± 80	30 ± 15	3.52
Cl 0024+16	0.39	2.4	13.2	125 ± 7	45 ± 5	2.5 ± 1.2	~ 6.3	1000 ± 70	30 ± 10	3.63
Cl 0054-27	0.58	0.25	16.8	230 ± 18	20 ± 7	5.2 ± 1.4	~ 9.4	1100 ± 100	30 ± 10	15.84